Published in final edited form as:
J Microelectromech Syst. 2006 February 1; 15(1): 223–236. doi:10.1109/JMEMS.2005.859083.

A Continuous-Flow Polymerase Chain Reaction Microchip With Regional Velocity Control

Shifeng Li [Member, ASME],
Department of Mechanical Engineering, The University of Texas at Austin, Austin, TX 78712 USA

David Y. Fozdar [Member, ASME],
Department of Mechanical Engineering, The University of Texas at Austin, Austin, TX 78712 USA

Mehnaaz F. Ali,
Department of Chemistry and Biochemistry, The University of Texas at Austin, Austin, TX 78712 USA.

Hao Li,
Department of Mechanical Engineering, Iowa State University, Ames, IA 50011 USA.

Dongbing Shao,
Department of Mechanical Engineering, The University of Texas at Austin, Austin, TX 78712 USA

Daynene M. Vykoukal,
Department of Molecular Pathology, The University of Texas M. D. Anderson Cancer Center, Houston, TX 77030 USA.

Jody Vykoukal,
Department of Molecular Pathology, The University of Texas M. D. Anderson Cancer Center, Houston, TX 77030 USA.

Pierre N. Floriano,
Department of Chemistry and Biochemistry, The University of Texas at Austin, Austin, TX 78712 USA.

Michael Olsen,
Department of Mechanical Engineering, Iowa State University, Ames, IA 50011 USA.

John T. McDevitt,
Department of Chemistry and Biochemistry, The University of Texas at Austin, Austin, TX 78712 USA.

Peter R.C. Gascoyne [Member, IEEE], and
Department of Molecular Pathology, The University of Texas M. D. Anderson Cancer Center, Houston, TX 77030 USA.

Shaochen Chen [Member, ASME]
Department of Mechanical Engineering, The University of Texas at Austin, Austin, TX 78712 USA

Shifeng Li: ; David Y. Fozdar: ; Mehnaaz F. Ali: ; Hao Li: ; Dongbing Shao: ; Daynene M. Vykoukal: ; Jody Vykoukal: ; Pierre N. Floriano: ; Michael Olsen: ; John T. McDevitt: ; Peter R.C. Gascoyne: ; Shaochen Chen: scchen@mail.utexas.edu

Abstract

Subject Editor A.P. Lee

This paper presents a continuous-flow polymerase chain reaction (PCR) microchip with a serpentine microchannel of varying width for "regional velocity control." Varying the channel width by incorporating expanding and contracting conduits made it possible to control DNA sample velocities for the optimization of the exposure times of the sample to each temperature phase while minimizing the transitional periods during temperature transitions. A finite element analysis (FEA) and semi-analytical heat transfer model was used to determine the distances between the three heating assemblies that are responsible for creating the denaturation (96 °C), hybridization (60 °C), and extension (72 °C) temperature zones within the microchip. Predictions from the thermal FEA and semi-analytical model were compared with temperature measurements obtained from an infrared (IR) camera. Flow-field FEAs were also performed to predict the velocity distributions in the regions of the expanding and contracting conduits to study the effects of the microchannel geometry on flow recirculation and bubble nucleation. The flow fields were empirically studied using micro particle image velocimetry (μ-PIV) to validate the flow-field FEA's and to determine experimental velocities in each of the regions of different width. Successful amplification of a 90 base pair (bp) *bacillus anthracis* DNA fragment was achieved.

Index Terms

Continuous-flow; microelectromechanical systems (MEMS); polymerase chain reaction (PCR); regional velocity control

I. INTRODUCTION

POLYMERASE chain reaction (PCR) is an assay used to amplify specific regions of DNA between two known flanking base pair sequences. PCR has become one of the most widely utilized scientific tools in molecular biology since its inception in the mid 1980s. Conventional PCR has revolutionized fields like molecular biology and biochemistry and has become an important tool in forensics, genetics, the evolutionary sciences, clinical research, and in many other areas [1]. Its applications range from diagnosis of infectious disease to analysis of specific gene mutations that occur in a variety of genetic disorders.

PCR amplification is obtained using short oligonucleotide primers which exactly complement the flanking sequences. Once attached to the host strands, the primers are extended by a DNA polymerase enzyme in the presence of deoxynucleoside triphosphates (dNTPs). Reaction conditions and heat transfer rates must be optimized for the PCR process to run most smoothly and efficiently. PCR can be conveniently divided into three distinct phases: denaturation (melting), annealing (hybridization), and extension (replication). In the denaturation phase, dsDNA (double-stranded DNA) is heated to approximately 85–98 °C so that the two strands of nucleotides divide into two single strands (ssDNA). Once the strands have separated, the temperature is cooled to 50–60 °C for the annealing phase where the primers hybridize to a flanking sequence on each ssDNA template. Finally, the temperature is increased to 70–75 °C and the target region is extended by means of a Taq polymerase enzyme starting from the flanking sequence and ending at the other end of the template. The Taq enzyme essentially extends the primers by pulling the dNTPs from the sample solution to complete the new copies of the target sequence. In contrast to denaturation and hybridization, which occur almost instantly, the length of the extension phase is restricted by the 100 nucleotide per second extension rate of the Taq enzyme. Theoretically, the time limiting factor for the reaction is the extension phase [2]. Realistically, the time constraining factor for the reaction involves limitations in the achievable heating and cooling rates of the sample.

In the past decade, microfabrication technology has led to the development of a variety of high-throughout miniature PCR microdevices. This technology has allowed for a drastic increase

in heat transfer rates due to the high surface area-to-volume ratio associated with microstructures. Such devices have been mainly constructed under two basic design platforms. The more common platform consists of etched microchambers in silicon that host immobilized (stationary) samples in contact with heating elements that cycle the temperature [3]–[6]. The other platform is based on a continuous-flow format where the sample is spatially cycled in a serpentine microchannel through three well-distinguished permanent temperature zones [7]–[15].

Since optimum reaction temperatures and exposure times of the sample to each temperature are key to successful DNA amplification, thermal/fluid control of heat transfer rates, temperature distributions, and sample velocities within the microchip and of the DNA sample are critical issues in PCR technology [16]. Typical problems associated with current flow-through PCR microdevices include: failure to maintain uniform temperatures in each of the three monolithic temperature zones due to lateral heat conduction between the heaters and unnecessarily extended transitional times, the periods in which the DNA sample is not at one of the three optimal phase temperatures (the region between the temperature zones). Obstacles like nonspecific amplification and low product yield typically arise from exceedingly long transitional times between the optimal temperatures of each phase and by unnecessarily extended exposure times to the high denaturation temperature. The way in which the heating and cooling of the samples is implemented in PCR is vital for high product yields and specificity. Although efforts have been made to study thermal/fluid transport phenomena within continuous-flow PCR devices, design approaches for better thermal/fluid control have not yet been explored [7]–[9].

Here we present a continuous-flow PCR microdevice with “regional velocity control” and a better heating configuration for the efficient chemical amplification of DNA. The microdevice contains a serpentine microchannel with varying widths serving to regulate the flow velocities of the DNA sample through the channel limiting transitional times, the time periods in which the sample is traveling between temperature zones (denaturation, annealing, and extension zones). Channel width variations were made by sets of periodically arranged expanding and contracting conduits. Finite element analysis (FEA) tools and a semi-analytical heat transfer model were used to investigate heat transfer and flow behavior within the microdevice and inside the serpentine microchannel. Specifically, the FEA02019;s were conducted to determine the optimal distances (heater spacings) between three integrated heating assemblies that generated the three monolithic temperature zones (see Fig. 1) and to predict the effects of the geometries of the expanding and contracting conduits on the flow fields in these regions. The semi-analytical heat transfer model was developed to predict the optimized heater spacings between the three heating assemblies. Results from the thermal FEA were compared with those from the semi-analytical heat transfer analysis to ensure precision of the optimized spacings. An experimental surface temperature distribution obtained by an infrared (IR) camera at the top surface of the microdevice opposite the side with the attached heating assemblies was taken to verify the accuracy of our predictions from both the thermal FEA and semi-analytical model. Microparticle image velocimetry (μ-PIV) was utilized to empirically visualize the velocity fields at various downstream locations within the microchannel. μ-PIV results were compared with the flow-field FEA to ensure the accuracy of determined flow velocities within segments of each of the various widths of the microchannel and to gauge the effects of the expanding and contracting channel geometries on flow recirculation and bubble nucleation. Successful amplification of a 90 bp DNA *bacillus anthracis* fragment was achieved using our PCR microchip.

II. DESIGN FEATURES/FABRICATION OF THE CONTINUOUS-FLOW PCR MICRODEVICE

In designing the continuous-flow PCR microdevice with regional velocity control, the following aspects were found to be very important: 1) microchip material selection, 2) serpentine microchannel geometry/dimensions (i.e., number of reaction cycles, length ratio—a ratio of the channel lengths traversing each temperature zone per geometrical thermal cycle), 3) microchip/heating assembly fabrication, and 4) heater spacings (the spacing between the temperature zones).

A. Microchip Material Selection

Polymers have been extensively used for biomedical microdevices since many are cheap biocompatible, and lend themselves to unique features which depend on the particular material and application [4], [6], [9]. However, because most polymers are highly permeable to gases, they are usually insufficient for use in PCR microdevices [6]. Silicon and glass have been the most widely used materials in lab-on-a-chip devices since a vast array of well-established integrated circuit (IC) and microfabrication technologies are available. The high thermal conductivity of silicon makes it difficult to maintain discrete well-regulated temperature zones due to lateral heat conduction and its opaque optical characteristics restrict the utilization of real-time fluorescence detection techniques. To the contrary, glass is an excellent choice for PCR microdevices since it is impermeable to gases, is readily treated by a variety of surface coating agents to reduce DNA and enzyme adsorption, is transparent to visible light making it amenable to fluorescence detection [17], and has a thermal conductivity suitable for establishing uniform temperature zones within a confined area while limiting lateral heat conduction.

B. Serpentine Microchannel Geometry and Heater Assembly Spacings

The geometry and arrangement of the serpentine microchannel with respect to the three temperature zones must ensure that the microchannel sufficiently traverses through each temperature zone, reduces the possibility for flow recirculation/bubble formation, and limits overall microchip dimensions. The layout of the channel must be consistent with the orientation and configuration of the heating assemblies. The velocity of a sample in a typical serpentine channel of constant cross-sectional area for PCR is the same throughout; velocities in both the transitional regions and temperature zones are monotonous. This results in unnecessarily extended denaturation, hybridization, and transitional periods that degrade enzyme activity and spawn the improper duplication of spurious DNA species. To eliminate these extended periods, the width of the microchannel in our flow-through chip was made variable in a periodic arrangement throughout its length by integrating expanding and contracting conduits, linear expansions and contractions in the side-walls of the microchannel. Small channel widths were set in the transitional zones so that the sample would have relatively high flow velocities in these regions. Larger widths were set in the temperature zones (denaturation, annealing, and extension) to provide for optimal exposure times. The dimensions of the channel were carefully chosen to avoid flow recirculation, which nucleates bubbles. The exposure time ratio of the sample to each temperature zone was decided to 1:2:4 for denaturation, hybridization, and extension, respectively. The widths for denaturation, hybridization, and extension (100 μm, 273 μm, and 340 μm, respectively) were predetermined by considering, to a close approximation, the relative exposure needs of commonly amplified DNA fragments. The channel width in the transition zones was set to 10 μm to coerce the sample through these interim regions at high velocities. The depth of the channel was maintained at 30 μm throughout its length so that the magnitude of the cross-sectional area was controlled by channel-width alone. To determine the channel-widths and microchannel length-ratio, the spacing between

the heaters was optimized to limit lateral heat conduction, which smears the temperature zones. Twenty identical channel oscillations (thermal cycles) for a 20-cycle PCR reaction were designed into the microchip. In addition to the normal reaction cycles, a preliminary extended melting cycle, providing for “hot start” PCR, and an extended post-extension cycle were appended to maximize replication.

C. Microchip/Heating Assembly Fabrication

To create the etched serpentine microchannel, a 100-nm amorphous silicon thin-film was initially deposited on a four-inch diameter borosilicate glass wafer. Amorphous silicon was chosen as the masking material due to its selective nature to the etchant [18]. After patterning, the channel was etched to 30 μm with hydrofluoric acid (HF) and stripped by reactive ion etching with CF_4 plasma. On a separate glass wafer, three holes of 1.0 mm diameter were powder blasted as inlets and outlets for access to the channel (additional assembly required). The patterned wafer and the separate glass piece with the holes were fusion bonded to the wafer with the serpentine microchannel.

To provide access to the channel, Headless Coned Nanoport Assemblies (UpChurch Scientific, N-126H, WA, USA) accommodating 0.79-mm (1/32-inch) tubing (OD) were bonded over the powder blasted holes on the upper wafer halve (after fusion bonding). Prior to affixation, the bottom surfaces of the Nanoports were soaked in isopropyl alcohol (IPA) for 5 min and the fused glass PCR microchip was cleaned in a Piranha solution (1600 ml H_2SO_4+800 ml H_2O_2) for 10 min. Both substrates were dried with N_2 gas and placed on a 100° C hot plate for 20 min to remove residual moisture. Two layers of a ring-shaped biocompatible epoxy were attached to each of the Nanoports to bind them to the glass directly superseding the holes. Alignment with the holes was achieved by threading a glass capillary of 0.4 mm diameter through the Nanoports and placing the far end of the capillary into the holes. The ports were positioned by letting them slide down the capillary directly onto the holes. Manual pressure was subsequently applied to the Nanoport to ensure complete adherence to the glass. The bond was made permanent by clamping the ports down while baking at 120° C for 90 min. The length, width, and thickness of the assembled chip measure 75, 48, and 1 mm, respectively.

Three heating assemblies, consisting of thin-film resistive Kapton Heaters (Minco, HK5160R157L12, MN, USA) appended to rectangular copper blocks, were integrated onto the chip to create the three discrete temperature zones. The copper blocks, measuring 60 mm long × 12 mm wide × 7 mm high, provided for more uniform temperature zones due to their lumped thermal capacitance and high thermal conductivity. The Kapton Heaters were bonded to the copper blocks using a single layer of a thermally conductive epoxy (Minco, PSA #10, MN, USA). The heater/copper block compilations were later applied to the glass substrate using two layers of the same adhesive. Thermocouples (Minco, S245PD12245, MN, USA) were cemented to each of the three copper blocks for temperature feedback via a connection to three digital PID (proportional, integral, and derivative) temperature controllers (Minco, CA16A2010-9502, MN, USA) and a homemade voltage amplification circuit. Schematics of the microchip assembly, devised mostly in Solid Works graphics software, are shown in Fig. 1; a photograph of the PCR microdevice is shown in Fig. 2.

III. THERMAL–FLUID ANALYSIS OF THE PCR MICRODEVICE

The optimized spacings between the heaters were determined using a finite element analysis (FEA) and semi-analytical heat transfer model. Results from the analyzes were compared to validate their accuracy and precision. Simulation results were also compared with empirically-obtained IR surface temperature data. An initial estimate of the geometry and dimensions of the microchannel was made from information found in prior literature. Using this information and noting that the optimal flow rate of the sample inside the microchannel was around 1 μl/

min, the thermal mass ratio of the DNA sample and the glass substrate per unit time was found to be less than 0.01 so the effect on the temperature distribution due to the convective heat transfer inside the microchannel was assumed to be negligible. The primary goal of the thermal investigations was to determine the size of the heater spacings in order to form finely tuned temperature zones while avoiding lateral heat conduction. A finite element simulation of fluid flow in the microchannel was also conducted to predict flow velocities and study the influences of the expanding and contracting conduits on flow recirculation and bubble nucleation. μ-PIV was used to take experimental flow-field measurements for comparison with the flow-field FEA.

A. Thermal Finite Element Analysis (FEA)

ANSYS 5.6 software was employed in the thermal FEA to optimize the spacings between the heaters. The following properties were used in the analysis: 1) the thermal conductivity of glass ≈ 1.13 W/m K and of the copper ≈ 400 W/m K and 2) the convective heat transfer coefficient with the air ≈ 7.5 $W/m^2 \cdot K$. The configuration of the three copper heating assemblies on the glass substrate is shown in Fig. 1.

To optimize channel geometry and to produce discreet temperature zones without lateral heat conduction, we investigated spacings ranging from 3 mm to 12 mm between juxtaposing heaters. The three heaters were positioned onto the bottom surface of the substrate and then adjusted in terms of the spacing between them. Temperature distributions in the *x*-direction with heater spacings of 3 mm-3 mm ("spacing between 96 °C and 72 °C"-"spacing between 72 °C and 60 °C"), 7–7.2 mm, and 12–12 mm are shown in Fig. 3. A spacing of 3 −3 mm was found to result in superfluous lateral heat conduction that partially smeared the temperature distribution between contiguous zones. Because of this, larger spacings were deemed necessary to enhance temperature zone isolation and uniformity. However, we found that some spacing confinement was necessary to keep the absolute size of the microchip to a minimum. Increasing the spacings does indeed improve zone isolation; however, it does so at the expense of increasing the dimensions of the microchip. Unnecessarily large heater spacings also result in increased flow distances required in the transitional regions between temperature zones (for a given heater width) elongating transitional periods. Heater spacings of 7.0 mm between the denaturation (96 °C) and extension (72 °C) zones and 7.2 mm between the extension and hybridization (60 °C) zones produced finely tuned temperature zones that were uniform and isolated with little lateral heat conduction.

The particular optimized heater spacings were derived by instilling a zero heat flux boundary condition in the y-direction at the leading edges of each of the heaters. Due to the 96 °C heater, a negative temperature gradient exists in the positive × direction. The presence of each heater creates a section of constant temperature with a size equal to the width of the heater. The heater used to create the extension zone was positioned first (middle heater) and the hybridization/annealing heater was positioned second (furthest from the 96 °C heater). Along the length of each of the second two heaters (i = 2,3), the heat flux in the vertical *y*-direction into the microchip varied due to disparities in the temperature difference between the superimposing differential heating element and the temperature of the underlying substrate. The "zero-heat-flux" boundary condition is the idea that the optimal positions for the heaters are located where the heat flux between the leading heating element of the lower temperature heaters (i = 2,3) and the underlying glass substrate (t_1)are zero. This is where the heater and the surface temperature are the same. By utilizing this condition and locating the complying positions, the heaters could be rearranged so that the leading edges of the two lower temperature heaters (72 °C and 60 °C) coincided with the locations with zero heat flux. As shown in Fig. 3, when the heater spacings were approximately 7 mm, the temperature zones were found to be isolated and uniform in the *x*-direction. At the same time, the absolute dimensions of the microchip

were minimized as much as possible. Temperature variation in the z-direction was very small so temperature in the z-direction was assumed uniform.

B. Semi-Analytical Thermal Modeling

A semi-analytical model was developed to verify the results of the thermal FEA. The analysis is based on the dimensions of the microchip and the material/thermal properties used in the thermal FEA. Convective heat transfer from the sides of the PCR chip was neglected due to the small exposed surface area and small temperature differences relative to the environment. This is equivalent to assuming that lateral heat flux is zero, dT/dx = 0, and that the temperature approaches the ambient temperature.

The analytical model was first devised by partitioning each heater into m equal divisions (m heating elements) as shown in Fig. 4 in order to study the heat flux between the heaters and the bottom surface of the substrate, which spatially varies in the x-direction. $w_{i,j}$, t_q,$h_{i,j}$ denote the width of the jth element heater, thickness of the glass slabs where $q = 1$ for t_1 and $q = 2$ for t_2, and interfacial positioning, respectively. Since two glass wafers were bonded together resulting in potential contact resistance between their interfaces (which is later neglected),$q = 1$ is the thickness of the bottom wafer in contact with the heaters and $q = 2$ is the thickness of the top wafer. The interfacial positioning and the position of a particular differential heating element are defined in Fig. 4. The two subscripts i and j denote specific values of h, i.e., the specific heating elements. The first subscript denotes the heater ($i = 1,2,3$) and the second subscript denotes the particular heating element within the heater ($j = 1,2,3,\ldots,m$). The i and j subscripts are the same on the heating element thickness variable,$w_{i,j}$.

A two-dimensional steady-state heat conduction equation for the bottom glass layer ($q = 1$)and the top glass layer ($q = 2$)was utilized to derive an (x,y) temperature distribution in the top slab.

$$\frac{\partial^2 T_q}{\partial x_q^2}+\frac{\partial^2 T_q}{\partial y_q^2}=0 \tag{1}$$

where q represents the qth glass layer referenced from the top surface of the microchip. At y = 0 we generated the following boundary conditions using an energy balance on a control volume incorporating a single rectangular heating element of width $w_{i,j}$:

$$\begin{gathered} -k_1\frac{\partial T_1}{\partial_y}|_{y=0}=-h_t(T_1-T_\infty)+\frac{Q_{i,j}}{w_{i,j}} \\ \text{for the } j \text{ th element heater on heater } i \text{ and} \\ -k_1\frac{\partial T_1}{\partial_y}|_{y=0}=-h_t(T_1-T_\infty) \\ \text{for regions (in the } x-\text{direction) without heaters} \end{gathered} \tag{2}$$

where $Q_{i,j}$ is the input power per unit length of element j on heater i($i = 1,2,3$), $w_{i,j}$ is the width of heating element j, and h_t is the convective heat transfer coefficient (we ignore the variation of h_t on the surfaces), and k_1 and k_2 are the thermal conductivities of the glass slabs.

If we define an input power function

$$\text{function } f(x)=\begin{cases} (Q_{i,j}/W_{i,j}) & \text{(for the j th element heater)} \\ 0 & \text{(for other regions)} \end{cases}$$

, (2) can be rewritten in a more general form as

$$-k_1 \frac{\partial T_1}{\partial y}|_{y=0} = -h_t(T_1 - T_\infty) + f(x). \tag{3}$$

The boundary conditions at the interface between $q = 1$ and $q = 2$, the bottom and top substrates, neglecting contact resistance are

$$-k_1 \left.\frac{\partial T_1}{\partial y}\right|_{y=t_1} = -k_2 \left.\frac{\partial T_2}{\partial y}\right|_{y=t_1} \quad \text{and} \quad T_1|_{y=t_1} = T_2|_{y=t_1}. \tag{4}$$

At the bottom of the PCR chip, we have

$$-k_2 \frac{\partial T_2}{\partial y}|_{y=t_1+t_2} = -h_t(T_2 - T_\infty). \tag{5}$$

Fourier transforms were utilized to morph the governing conduction equation and the boundary conditions forming an eigenvalue problem [19]. The general solution to the eigenvalue problem, consisting of $A_q \sinh(\lambda y_q)$ and $B_q \cosh(\lambda y_q)$ terms, was applicable to both the and q = 1 and q = 2 layers. The transformed boundary conditions were used to evaluate A_1, B_1 for q = 1 and A_2, B_2 for q = 2. The temperature distribution for the q = 1 layer was found to be the following:

$$T_1(x, y_1) - T_\infty = \frac{1}{2\pi} \int_{-\infty}^{+\infty} \frac{F(\lambda)}{h_t \zeta_1 - k_1 \lambda} \times [\sinh(\lambda y_1) + \zeta_1 \cosh(\lambda y_1)] e^{i\lambda x} d\lambda \tag{6}$$

where

$$F(\lambda) = \sum_{i=1}^{3} \sum_{j=1}^{m} \frac{Q_{ij}}{w_{i,j}} \frac{\exp(-i\lambda x_{i,2}) - \exp(-i\lambda x_{i,1})}{-i\lambda} \quad \text{and}$$

$$\varsigma_1 = B_1 / A_1$$

The x-dependent temperature distribution at the interface between the q = 1and q = 2 layers was found to be

$$T_2(x, y = t_1) - T_\infty = \frac{1}{2\pi} \int_{-\infty}^{+\infty} \frac{F(\lambda)}{h_t \zeta_1 - k_1 \lambda} \times [\sinh(\lambda t_1) + \zeta_1 \cosh(\lambda t_1)] e^{i\lambda x} d\lambda. \tag{7}$$

Equation (6) was further evaluated by expanding it into an equivalent linear combination of $3m$ analytical equations, one corresponding to each heating element j for the three heaters i = 1,2,3. Thus, a matrix of equations was formulated and solved computationally for a comprehensible (x, y_1) temperature distribution and the generated power $Q_{i,j}$ by each heating element. By differentiating (6) with respect to the y-direction, we obtained the following temperature gradient equation:

$$\frac{\partial T(x,y_1)}{\partial y_1} = \frac{1}{2\pi}\int_{-\infty}^{+\infty} \frac{F(\lambda)}{h_{t\zeta 1} - k_1\lambda} \times [\lambda \cosh(\lambda y_1) + \lambda\zeta_1 \sinh h(\lambda y_1)] e^{i\lambda x} d\lambda. \quad (8)$$

In accordance with the "zero heat flux" criterion whereby the heat flux at the leading edges of the extension (72 °C) and hybridization (60 °C) heaters should be zero at y = 0 (surface with the heaters), (8) was set equal to zero for $y = y_1 = 0$ and solved for the two heating elements $h_{i,1}$where $i = 2,3$.

$$\left.\frac{\partial T(i=2,j=1)}{\partial y_1}\right|_{y=0} = 0$$
$$\left.\frac{\partial T(i=3,j=1)}{\partial y_1}\right|_{y=0} = 0. \quad (9)$$

From (9), the heater spacings were determined. We found heater spacings of 7.0 mm between the denaturation and extension zones and 7.2 mm between the extension and hybridization zones produce nicely regulated temperature zones without lateral heat conduction problems.

C. Infrared (IR) Surface Temperature Measurements

Since the components of the PCR cocktail (mixture) and amplification reaction are temperature-sensitive, it was important to know, at least to a rough estimate, the temperature in the channel so that the thermocouples could be calibrated and the set points on the PID (proportional, integral, and derivative) controllers could be adjusted properly. Therefore, surface temperatures were measured at the top surface of the microchip and used as a baseline for determining temperatures within the microchannel. An infrared (IR) camera was used to measure surface temperatures. Before any measurements were taken, the IR camera was calibrated to compensate for the effects of the environment, i.e., the emissivity was determined and accounted for, etc. After the temperature readings stabilized, the surface emissivity was measured using a TrueRMS Supermeter (HHM290, OMEGA, USA) so the value could be inputted into the camera. An IR image showing the experimental surface temperature distribution is shown in Fig. 5. Temperatures at locations in the direction of the thickness of the chip (y-direction) were estimated using the IR surface temperature measurements (at $y = t_1 + t_2$) as a reference. The heater spacings and temperature profiles in the x-direction predicted by our semi-analytical model and FEA matched those from the IR measurement as shown in Fig. 6. The discrepancies in temperature at the edges of the microchip between the FEA and semi-analytical model are due to the infinite boundary assumption as was discussed earlier.

D. Flow Simulations Within the Serpentine Microchannel

It was hypothesized that having a serpentine channel of varying widths could potentially cause flow recirculation that would nucleate bubbles in the regions with the expanding and contracting conduits [10]. Bubbles induce temperature gradients within the sample that significantly reduce or inhibit amplification while flow recirculation increases flow resistance (and may nucleate bubbles). Flow recirculation occurs when the back pressure supersedes the pressure drop in the flow direction resulting in forward and backward flows within different regions of the cross-section. The maximum *Re* number for the flow in the microchannel of our microchip was 18 at typical flow rates in our experiments (1–5 μl/min).

The fluid in the channel was observed to be highly constricted in some instances without lingering obstructions blocking the flow. Flow recirculation caused by both excessive back pressure and microchannel geometry was thought to be the culprit. If a reasonable pressure

drop exists in the downstream direction, then it is highly improbable that flow recirculation will occur. Oppositely, adverse pressure gradients (backpressure) are much more likely to induce some recirculation regimes near the microchannel wall.

It was found in the literature that when the angles of the converging/ diverging conduits were small, the probability of flow recirculation is minimized vis-à-vis steep profiles. Furthermore, an angle of 7° was found to be the best wall profile slope of the conduit expansions and retractions for minimizing recirculation effects [20]. Fig. 7 shows colorimetric velocity fields given by the FEA inside the expanding and contracting conduits within the microchannel.

E. μ-PIV Velocity Field Measurements

Micro particle image velocimetry (μ-PIV) was used to measure the velocity fields inside the microchannel at various downstream locations [21]–[23]. A double pulsed 532 nm Nd:YAG laser beam (Continuum, Santa Clara, CA), attenuated to 3 mJ/pulse, was utilized in the measurements. 900 nm diameter fluorescent seed particles (Duke Scientific Co., Palo Alto, CA) absorbed the laser light and emitted at a peak excitation wavelength of 612 nm. The emitted light was filtered and imaged with an inverted biological microscope (Nikon model T-300 Inverted Microscope). A La Vision Flowmaster 3 camera (Lavision Inc., Ypsilanti, MI) was used to capture the μ-PIV image pairs for cross-correlation analysis.

The concentration of the fluorescent particle solution was prepared so that a sufficient number of seed particles would fall within the depth-of-correlation [24], [25] in each region of the microchannel that measurements were taken. This resulted in a volumetric particle concentration of approximately 0.057% of the total volume of solution. This volume fraction of seed particles was small enough that any two-phase solid/liquid effects were negligible and that the working fluid could be considered a single-phase fluid.

Error in the μ-PIV images was estimated by assuming that the measured particle displacements for velocity calculations were accurate to within approximately a tenth of the seed particle image diameter [26]. For the μ-PIV experiments, the image diameter for a particle in the object plane can be approximated as [27]

$$d_e=(M^2d_p^2+d_s^2)^{1/2} \tag{10}$$

where M is the magnification,d_p is the particle diameter, and d_s is the diffraction-limited spot size. When d_e = 1.9 μ m, the measured particle displacement in the μ-PIV experiments were accurate to within 0.19 μm. In each of the μ-PIV experiments, the particles moved approximately 7 μm between laser pulses resulting in an experimental uncertainty of 2.7%.

To reduce the amount of uncertainty associated with the experiment, 100 images were obtained, summarized, and averaged to return a velocity profile inside the microchannel for each measurement location. Flow rates of 1 μl/min and 5 μl/min were used in the μ-PIV measurements. Velocity measurements were obtained at 16 locations in the downstream direction where flow recirculation was thought to most likely occur. The 16 positions were located along a single cycle of the microchannel geometry. The measurements taken for the individual cycle were representative of the flow field in the entire microchannel due to its periodic geometry.

Fig. 8 shows μ-PIV images taken at locations where the velocity of the fluid was the fastest and at regions containing expanding and contracting conduits. Fig. 9 shows velocity profiles in the three temperature zones at a flow rate of 1 μl/min. The average velocities in the denaturation, hybridization, and extension zones were found to be 4.46 mm/s, 2.36 mm/s, and

1.73 mm/s, which were close to the average velocities of 3.78, 1.74, and 1.44 mm/s, respectively, obtained from the FEA. Exposure times of the sample to each temperature per cycle were calculated by dividing the total volume of the segment by the average volume flow rate of the particular segment. The exposure time ratio of the three temperature zones was calculated to be 1:2:4 from the μ-PIV measurements. It was also seen that there was very little flow recirculation in the microchannel at the tested flow rates.

IV. PCR AMPLIFICATION EXPERIMENTS

The experimental setup for PCR amplification is shown in Fig. 10. A 100 μl gas-tight syringe (Hamilton Company, UK) was connected to a programmable syringe pump (Ne-1000, New Era Pump System, NY). The syringe pump was connected to the PCR chip using PEEK tubing (UpChurch, WA). In order to avoid channel blockage, an in-line 0.5 μm micro-filter (UpChurch, WA) was installed in front of the glass chip to remove particulate residuals inside the solution. A 90 bp *bacillus anthracis* sequence (from Sterne) strain was used to test the PCR chip. The upstream DNA primer was 5‘AATCTTCCGCAATGGACG3’ and the downstream primer was 5‘TTCTTCCCTAACAACAGAG3’. Initially, deionized (DI) water and ethanol were flushed through the microchannel at a flow rate of 10 μl/min. SigmaCote (Sigma, USA) was used to silanize the inner wall of the microchannel to prevent the adsorption of Taq enzyme to the surface of the microchannel. After silanization, ethanol was used to remove excess silane and DI water was once again flushed through the microchannel at a flow rate of 10 μl/min. The heating elements were then turned on and allowed to stabilize. At this point, liquid buffer was pumped through the chip at a flow rate of 1 μl/min to prime the channel. The buffer contained 5 μg/ μl and 10% Tween 20 surfactant. 100 μl DNA sample was then pumped through the microchannel at a flow rate of 1 μl/min and the amplified product was collected from the outlet in 15 μl aliquots and placed in small vials for further analysis using slab-gel electrophoresis. A negative control was run without enzyme to make sure that the amplified product was specific. Fig. 11 shows the results from gel electrophoresis. The leftmost lane (lane 1) is the DNA ladder, which was used to determine whether amplified sequence was of the proper length. Lanes 2–4 show the highly amplified DNA sequence obtained from the PCR microdevice. The rightmost lane (lane 5) shows the control sequence. The control was used to rule out erroneous amplification and was devoid of the Taq enzyme.

V. CONCLUSION

We have developed a continuous-flow PCR microchip with a serpentine microchannel of varying widths and optimized heater spacings for optimal DNA amplification. Varying the channel widths allowed control over the local velocities at different downstream positions in the microchannel thereby optimizing the exposure times of the sample to each temperature zone and significantly reducing transitional periods. A semi-analytical heat transfer model and FEA were performed to calculate the temperature distribution inside the microchip and to optimize the spacings between the heaters. Empirical IR surface temperature measurements showed that the temperature zones were uniform. The IR measurements agreed with results from the semi-analytical model and the thermal FEA and were used as a baseline in determining the empirical temperatures within the microchip. μ-PIV was utilized to visualize the velocity fields inside the microchannel at different downstream locations. Results of the μ-PIV measurements were compared with the flow-field FEA. Successful amplification of a 90 bp *bacillus anthracis* DNA fragment was achieved.

ACKNOWLEDGMENT

S. Chen appreciated useful discussion with Dr. T. Mautner in Navy Spawar Systems Center, San Diego, CA, and Dr. K. Alder-Storthz from the University of Texas Health Science Center-Dental Branch, Houston, TX. S. Li appreciated

valuable discussion with Q. Hao from the Massachusetts Institute of Technology (MIT), Cambridge, about analytical modeling of heat transfer inside the PCR microchip.

This work was partially supported by the U.S. Department of Defense (N66001-03-1-8939) and a seed grant from the University of Texas at Austin.

REFERENCES

1. Mullis KB. The polymerase chain-reaction (nobel lecture). Angewandte Chemie-International Edition in English 1994;vol. 33:1209–1213.
2. Wittwer CT, Ririe KM, Andrew RV, David DA, Gundry RA, Balis UJ. The lightcycler(TM) a microvolume multisample fluorimeter with rapid temperature control. Biotechniques 1997;vol. 22:176–181. [PubMed: 8994665]
3. Lin YC, Huang MY, Young KC, Chang TT, Wu CY. A rapid micro-polymerase chain reaction system for hepatitis C virus amplification. Sensors and Actuators B-Chemical 2000;vol. 71:2–8.
4. Hong JW, Fujii T, Seki M, Yamamoto T, Endo I. Integration of gene amplification and capillary gel electrophoresis on a polydimethyl-siloxane-glass hybrid microchip. Electrophoresis 2001;vol. 22:328–333. [PubMed: 11288901]
5. Lagally ET, Emrich CA, Mathies RA. Fully integrated PCR-capillary electrophoresis microsystem for DNA analysis. Lab. on a Chip 2001;vol. 1:102–107. [PubMed: 15100868]
6. Shin YS, Cho K, Lim SH, Chung S, Park SJ, Chung C, Han DC, Chang JK. PDMS-based micro PCR chip with parylene coating. J. Micromechan. Microeng 2003;vol. 13:768–774.
7. Li S, Chen S. Design, simulation, and micro-fabrication of integrated, heat-conduction based DNA chip. J. Manufact. Process 2003;vol. 6:24–31.
8. Chen ZY, Qian SZ, Abrams WR, Malamud D, Bau HH. Thermosiphon-based PCR reactor: Experiment and modeling. Anal. Chem 2004;vol. 76:3707–3715. [PubMed: 15228345]
9. Hashimoto M, Chen PC, Michell MW, Nikitopoulos DE, Soper SA, Murphy MC. Rapid PCR in a continuous flow device. Lab. on a Chip 2004;vol. 4:638–645. [PubMed: 15570378]
10. Schneega I, Kohler JM. Flow-through polymerase chain reactions in chip thermocyclers. Rev. Mole. Biotechnol 2001;vol. 82(12):101–121.
11. Schneegass I, Brautigam R, Kohler JM. Miniaturized flow-through PCR with different template types in a silicon chip thermocycler. Lab. on a Chip 2001;vol. 1:42–49. [PubMed: 15100888]
12. Chou CF, Changrani R, Roberts P, Sadler D, Burdon J, Zen-hausern F, Lin S, Mulholland A, Swami N, Terbrueggen R. A miniaturized cyclic PCR device-modeling and experiments. Microelectron. Eng 2002;vol. 61(2):921–925.
13. Liu J, Enzelberger M, Quake S. A nanoliter rotary device for polymerase chain reaction. Electrophoresis 2002;vol. 23:1531–1536. [PubMed: 12116165]
14. Kopp MU, de Mello AJ, Manz A. Chemical amplification: Continuous-flow PCR on a chip. Science 1998;vol. 280:1046–1048. [PubMed: 9582111]
15. Obeid PJ, Christopoulos TK, Crabtree HJ, Back-house CJ. Microfabricated device for DNA and RNA amplification by continuous-flow polymerase chain reaction and reverse transcription-polymerase chain reaction with cycle number selection. Anal. Chem 2003;vol. 75:288–295. [PubMed: 12553764]
16. Yoon DS, Lee YS, Lee Y, Cho HJ, Sung SW, Oh KW, Cha J, Lim G. Precise temperature control and rapid thermal cycling in a micromachined DNA polymerase chain reaction chip. J. Micromechan. Microeng 2002;vol. 12:813–823.
17. Obeid PJ, Christopoulos TK. Continuous-flow DNA and RNA amplification chip combined with laser-induced fluorescence detection. Analytica. Chimica. Acta 2003;vol. 494:1–9.
18. Simpson PC, Woolley AT, Mathies RA. Microfabrication technology for the production of capillary array electrophoresis chips. Biomed. Microdev 1998;vol. 1:7–26.
19. Hao Q. Analytical heat-transfer modeling of multilayered microdevices. J. Micromechan. Microeng 2004;vol. 14:914–926.
20. Japikse D, Baines NC. Diffuser design technology. Concepts ETI. 1998
21. Meinhart CD, Wereley ST, Santiago JG. PIV measurements of a microchannel flow. Exp. Fluids 1999;vol. 27:414–419.

22. Devasenathipathy S, Santiago JG, Wereley ST, Meinhart CD, Takehara K. Particle imaging techniques for microfabricated fluidic systems. Exp. Fluids 2003;vol. 34:504–514.
23. Li H, Olsen MG. MicroPIV measurements in square microchannels with hydraulic diameters from 200 mm to 640 mm. Int. J. Heat Fluid Flow. AUTHOR: PLEASE UPDATE, IF POSSIBLE—ED., to be published
24. Olsen MG, Adrian RJ. Brownian motion and correlation in particle image velocimetry. Opt. Laser Technol 2000;vol. 32:621–627.
25. Bourdon CJ, Olsen MG, Gorby AD. Validation of analytical solution for depth of correlation in microscopic particle image velocimetry. Measure. Sci. Technol 2004;vol. 15:318–327.
26. Prasad AK, Adrian RJ, Landreth CC, Offutt PW. Effect of resolution on the speed and accuracy of particle image velocimetry interrogation. Exp. Fluids 1992;vol. 13:105–116.
27. Adrian RJ, Yao CS. Pulsed laser technique application to liquid and gaseous flows and the scattering power of seed material. Appl. Opt 1983;vol. 24:42–52.

Biographies

Shifeng Li received the M.S. and Ph.D. degree from Iowa State University, Ames, and The University of Texas at Austin in 2001 and 2004, respectively.

During his years at Iowa State University and the University of Texas at Austin, he conducted research on development of microfluidic systems for biomedical applications, such as PCR and protein/DNA detection. In March 2005, he joined the Mass Group of the University of Illinois as a Postdoctoral Researcher. His research interests cover microfluidic, lab-on-a-chip, and MEMS for nanobiotechnology. He is author or coauthor of 18 papers.

Dr. Li received the Jin Fu Fellowship in 1991 and Continuity Fellowship 2004. He is a Member of the American Society of Mechanical Engineers (ASME).

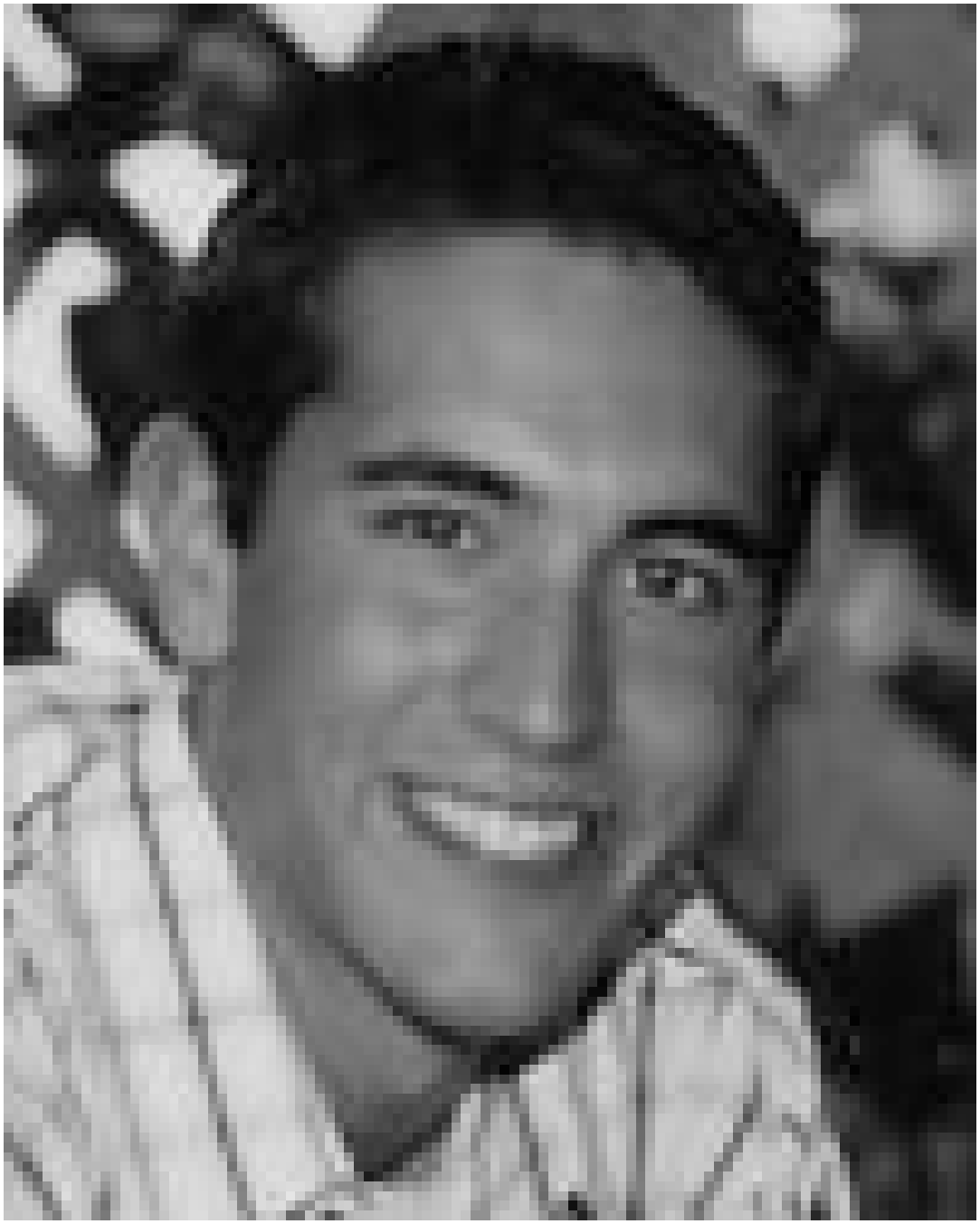

David Y. Fozdar received the B.S.E. degree in mechanical engineering from the University of Oklahoma in 2003 and the M.S.E. degree in mechanical engineering from The University of Texas at Austin in 2005. Currently, he is pursuing the Ph.D. degree in mechanical engineering at The University of Texas at Austin, where he is serving as a graduate research assistant for Dr. S. Chen. His B.S.E. degree was conferred with “Special Distinction” by the faculty at the University of Oklahoma.

His research interests lie Lab on a chip technologies, the use of ultrafast lasers in micro/nanomachining and biomedical applications, and soft-polymer fabrication.

Mr. Fozdar received the College of Engineering Thrust 2000 Endowed Graduate Fellowship at The University of Texas at Austin and Honorable Mention in the 2005–2006 National Science Foundation Graduate Research Fellowship Program. He is a member of the American Society of Mechanical Engineers (ASME).

Mehnaaz F. Ali was born in Calcutta, India, in 1976. She received the B.S. degree in biochemistry from the University of Texas at Austin in 2000. She is currently working toward the Ph.D. degree in chemistry under the supervision of Prof. J. T. McDevitt.

She is the recipient of the Dorothy B. Banks Research Fellowship at the University of Texas at Austin. Her current research efforts are directed toward the development of a chip-based sensor array that is suitable for the real-time detection of oligonucleotides.

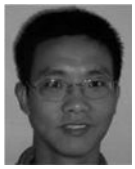

Hao Li received the B.S. and M.S. degrees in mechanical engineering from Shanghai Jiao Tong University, Shanghai, China, in 1996 and 1999, respectively, and is currently working toward the Ph.D. degree in mechanical engineering at Iowa State University, Ames.

He worked at Carrier Air-Conditioner, Co., Ltd., and Spirax Sarco Engineering, Co., Ltd., in China, before pursuing the Ph.D. degree. He is currently a Research Assistant in Iowa State University. His research interests include microfluidic system design and fabrication using photolithography, experimental laminar, transitional, and turbulent microfluidics using microscale particle image velocimetry technology, heat transfer, and temperature measurement using fluorescent dyes.

Dongbing Shao received the B.E. degree from Tsinghua University, China, and the M.S. degree in mechanical engineering from University of Colorado at Boulder. He is working towards the Ph.D. degree in mechanical engineering at The University of Texas at Austin.

He is currently working in the area of nanofabrication and nanophotonics.

Daynene M. Vykoukal received the B.S. degree in biochemistry from Texas A&M University, College Station, in 1994 and the Ph.D. degree in cell and molecular biology from Baylor College of Medicine, Houston, TX, in 2001.

Currently, she is a Postdoctoral Fellow in the Department of Molecular Pathology at the University of Texas M. D. Anderson Cancer Center, Houston. Her research interests include the use of biochemical assays in microsystems and the development of lab-on-a-chip-based technologies for molecular diagnostics.

Jody Vykoukal received the Ph.D. degree in biophysics from The University of Texas Graduate School of Biomedical Sciences at Houston in 2001.

Since 1993, he has been at The University of Texas M. D. Anderson Cancer Center in Houston, where he is currently a Research Associate in the Department of Molecular Pathology. His research interests include the application of dielectrophoresis to the separation and analysis of biological and biochemical analytes, particularly in fluidic microsystems.

Pierre N. Floriano was born in Besançon, France, in 1970. After he received the Diplôme d'Etudes Universitaires Générales (D.E.U.G.) in mathematics, physics, and chemistry in 1991, he received the License and Maîtrise in chemistry and applied electrochemistry, in 1992 and 1993, respectively, at the same university. He completed his French education with a Dipl̂me d'Etudes Approfondies (D.E.A.) in physical chemistry in May 1994. He received the Ph.D. degree in analytical/physical chemistry in May 2001 at Louisiana State University, Baton Rouge.

He served in the French Army from 1994 to 1995, and then came to the United States. He was a Postdoctoral Fellow with Prof. J. T. McDevitt at the University of Texas at Austin for two years. He is continuing on as a Research Scientist involved with the development of microfluidic diagnostic platforms, pattern recognition, and data analysis algorithms.

Michael Olsen received the B.S., M.S., and Ph.D. degrees from the University of Illinois at Urbana-Champaign in 1992, 1995, and 1999.

Upon completion of his doctorate, he was a Postdoctoral Research Associate at the Beckman Institute for Advanced Science and Technology working on microfluidic mixing and microscopic particle image velocimetry. In 2000, he joined the faculty of Iowa State University as an Assistant Professor of Mechanical Engineering. His area of expertise is experimental fluid mechanics, particularly laser-based measurement techniques such as particle image velocimetry and planar laser induced fluorescence. His current research interests include microscale fluid phenomena, turbulent mixing, and Taylor–Couette flows.

John T. McDevitt received the B.S. degree in chemistry from California Polytechnic State University, San Luis Obispo, in 1982. There he was distinguished with the Chemistry Department Research Award. He received the Ph.D. degree in chemistry from Stanford University, Stanford, CA, in 1987 and was honored with a prestigious Grace Fellowship.

He then completed postdoctoral research at the University of North Carolina at Chapel Hill. In September 1989, he accepted a position as Assistant Professor of Chemistry at University of Texas-Austin. He was promoted to Associate Professor with tenure in September of 1995 and to Full Professor in the Fall semester of 2000. In 1996, he developed the concept for and launched a research program directed toward a microchip-based technology suitable for the rapid analysis of complex fluids. This work was selected as part of Science Coalition's Best Scientific Advances for the Year. To date, these microchip sensors have been shown to be suitable for detection/quantification of acids, bases, salts, sugars, proteins, viruses, and DNA oligomers. Likewise, the chemical and biochemical content of complex fluids such as blood and urine can be digitized in near-real-time. Work is now in progress to correlate these "digital fingerprints" with important global health care, environmental, biomedical, homeland security and food safety/quality application areas. Recently, Prof. McDevitt has helped to launch a new company called LabNow based on this same microchip sensor technology for HIV monitoring applications for use in resource poor settings. At the University of Texas-Austin, he has published over 140 papers in scientific journals and has secured over 75 patents/patent applications.

Dr. McDevitt, he received the Presidential Young Investigator Award and in 1991 was granted the Exxon Education Foundation Award in 1990.

Peter R. C. Gascoyne (M'00) received the Ph.D. degree in electronic materials science from The University of Wales, Bangor, U.K., in 1979.

He is a Professor in the Department of Molecular Pathology at The University of Texas M. D. Anderson Cancer Center, Houston, TX. His research interest is the application of dielectric methods to cell analysis and sample manipulations in microfluidic diagnostic systems. He is the author of more than 80 publications and an inventor on more than 20 patents.

Dr. Gascoyne has been a Member of the IEEE Engineering in Medicine and Biology Society (EMBS) for 15 years.

Shaochen Chen received the Ph.D. degree in mechanical engineering from the University of California, Berkeley, in 1999.

Currently, he is an Associate Professor with the Mechanical Engineering Department at the University of Texas at Austin. His research interest lies in MEMS/NEMS, nano-and microscale laser materials processing, and thermal/fluid transport in MEMS/NEMS. He teaches a graduate course, ME381R-“MEMS/NEMS” at the University of Texas at Austin.

Dr. Chen received the CAREER award from the U.S. National Science Foundation in 2001, the Outstanding Young Manufacturing Engineer award from the Society of Manufacturing

Engineers in 2002, and the Young Investigator award from the U.S. Office of Naval Research in 2004. He is a committee member of ASME Nanotechnology Institute and IEEE Nanotechnology Council. He is also on the Technical Committee for NEMS/MEMS packaging of the Electronics and Photonics Packaging division (EPPD) of ASME. He served as a Guest Editor in 2003 for IEEE Transactions on Advanced Packaging: *Special Issue on NEMS/MEMS Packaging*. He is a member of the American Society of Mechanical Engineers (ASME).

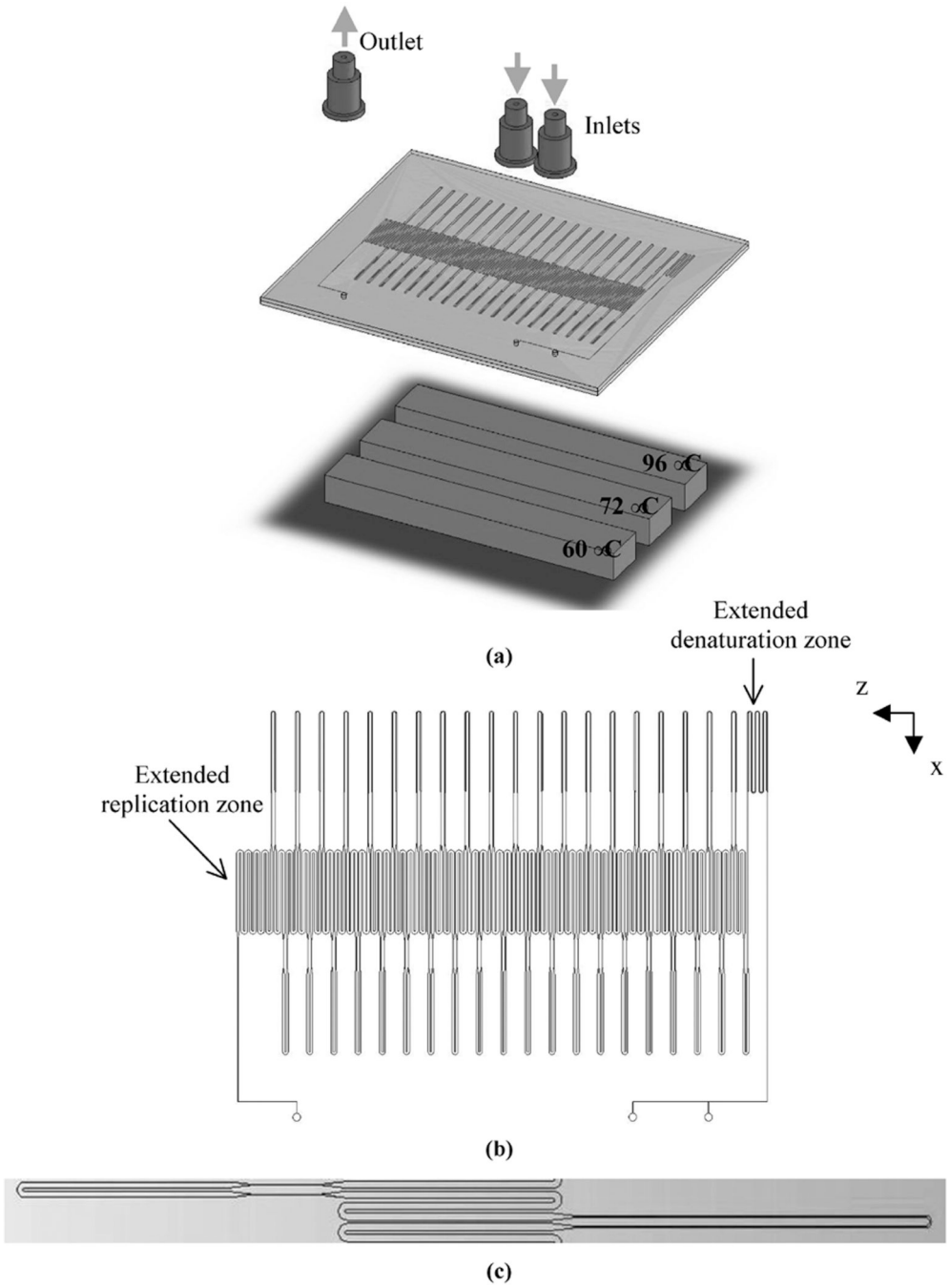

Fig. 1.
(a) A schematic of the thermally-optimized 20-cycle continuous-flow PCR microdevice with "regional velocity control". (b) A top view of the microchip (mask). (c) One cycle of the microchannel showing the varying widths.

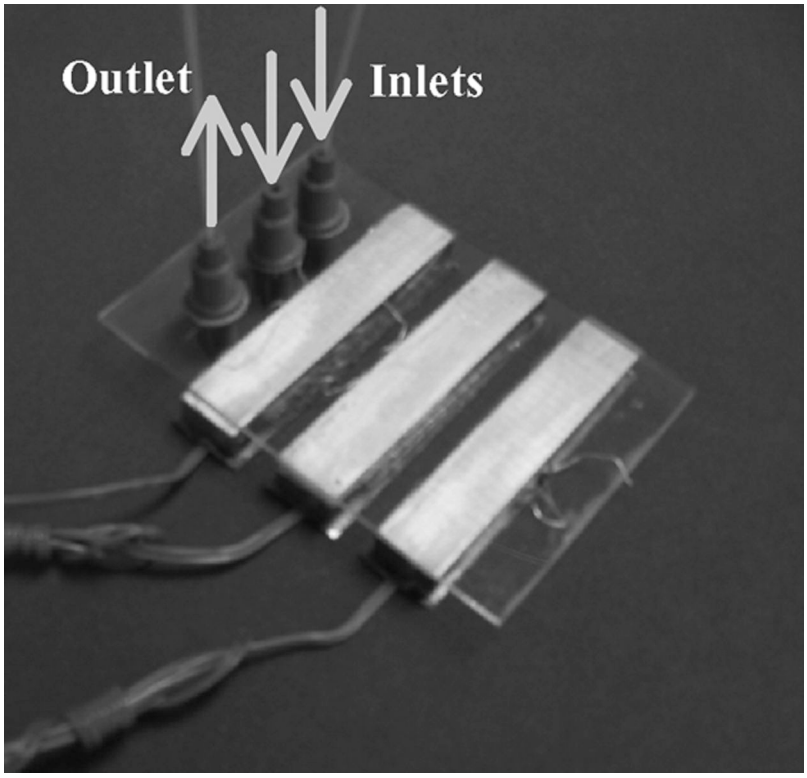

Fig. 2.
Photograph of the 20-cycle PCR microdevice.

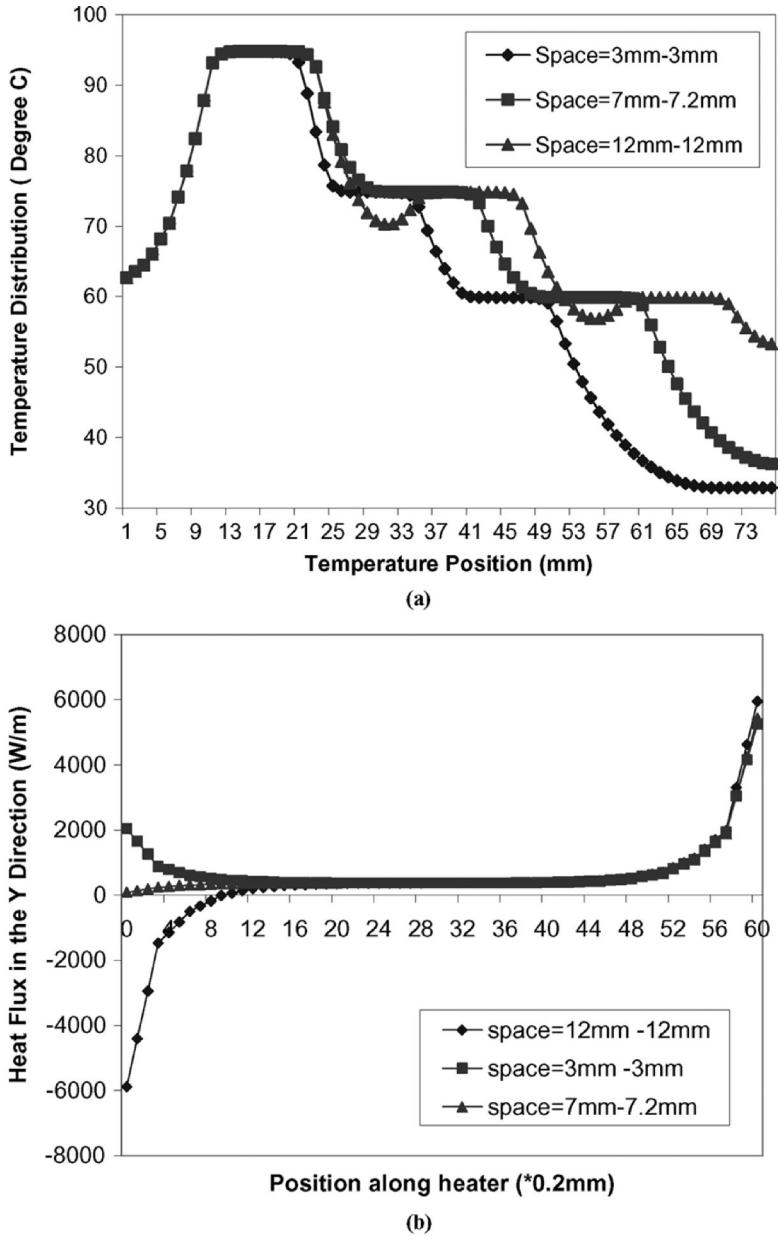

Fig. 3.

(a) Temperature distributions in the x-direction from 96 °C to 72 °C to 60 °C at various heater spacings. Spacings of approximately 7 mm resulted in temperature zones that were well isolated. (b) Heat flux in the vertical direction at heater spacings of 3–3 mm, 7–7.2 mm, and 12–12 mm.

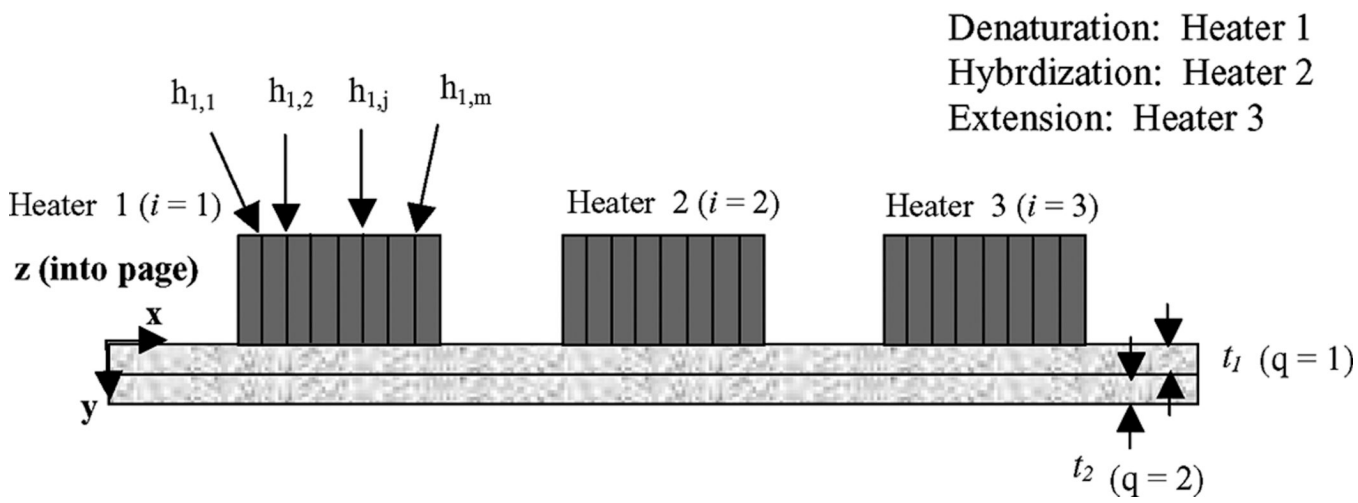

Fig. 4.

The inverted (oriented upside down) geometry serving as the basis for our semi-analytical model of thermal behavior in the PCR microchip. The configuration was also used in the "zero-heat-flux" condition in the thermal FEA.

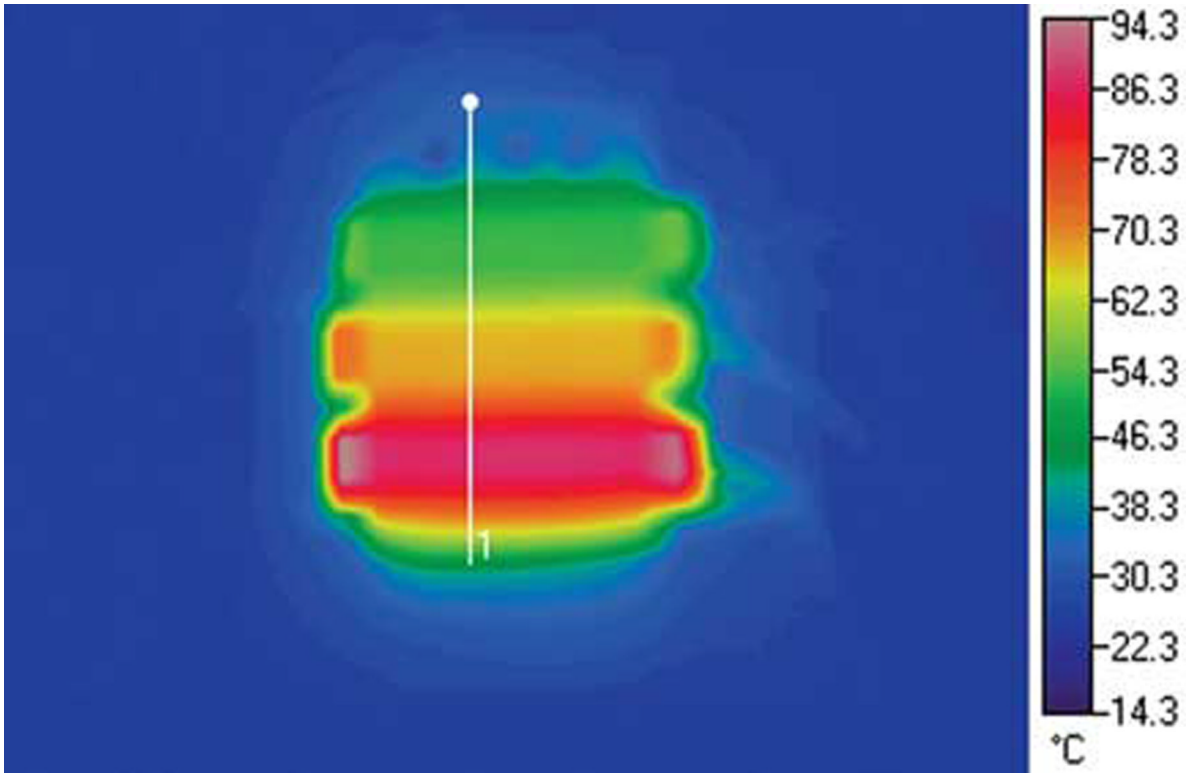

Fig. 5.
An IR picture showing the temperature distribution on the top surface of the microchip (opposite the side in contact with the three heating assemblies).

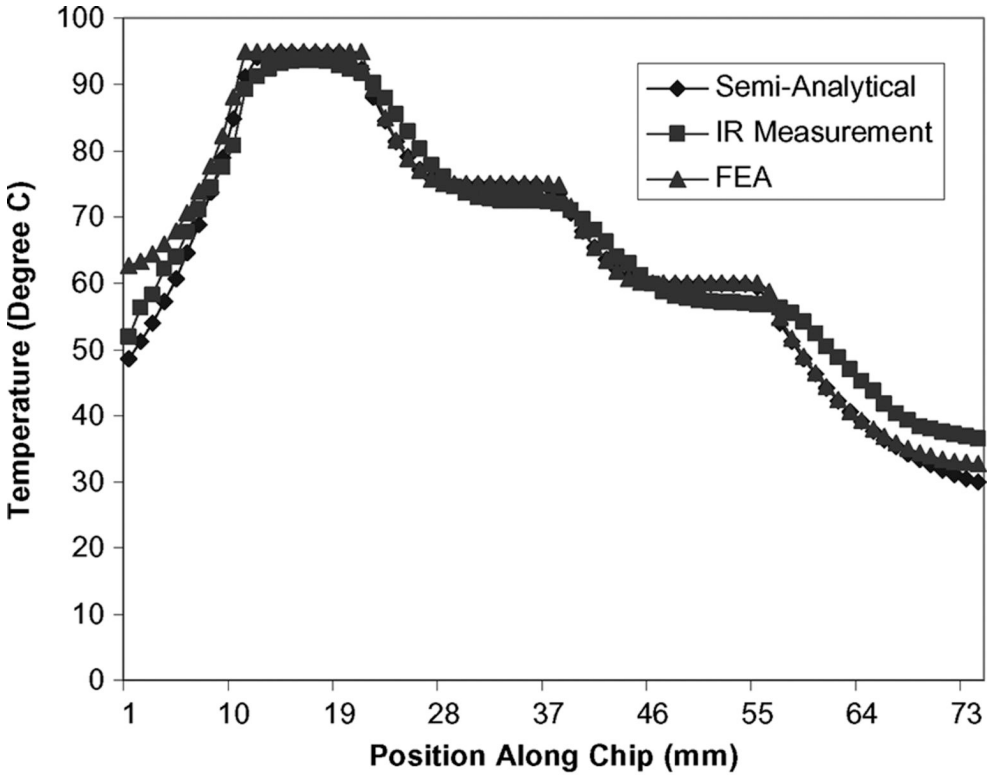

Fig. 6.
Temperature profiles along the x-direction extracted from the semi-analytical model, finite element analysis, and IR measurement.

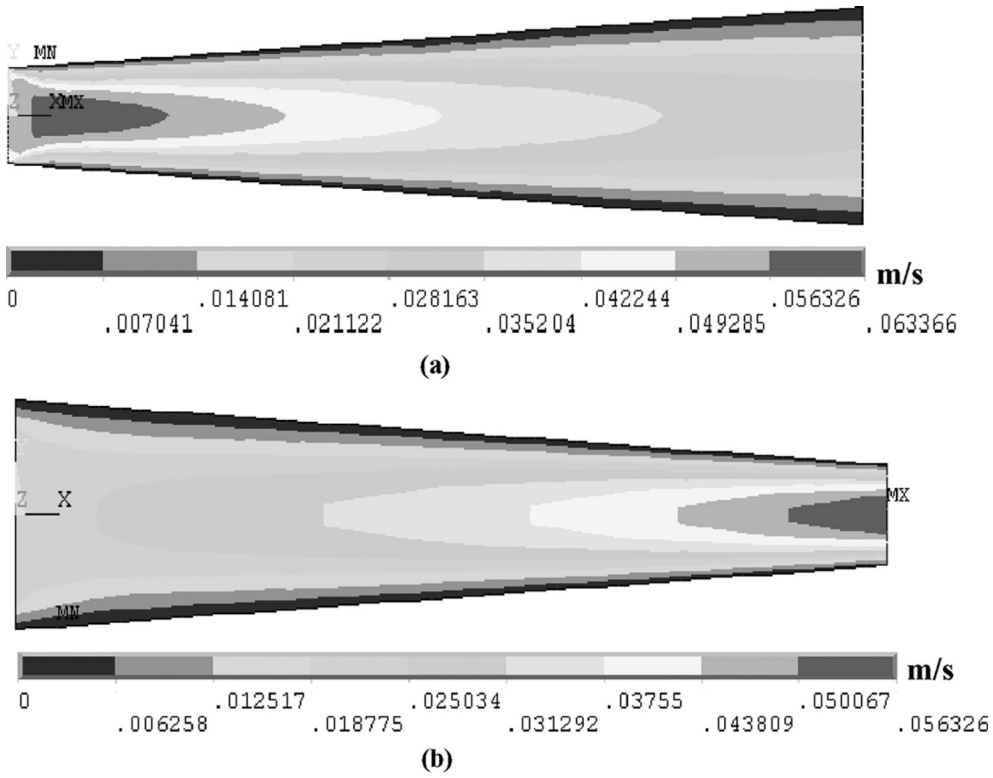

Fig. 7.

Velocity field distributions of an (a) 7° diffuser (expansion) and a (b) 7° nozzle (contraction) at the target flow rate of 1–5 μl/min. The distributions were produced by ANSYS software.

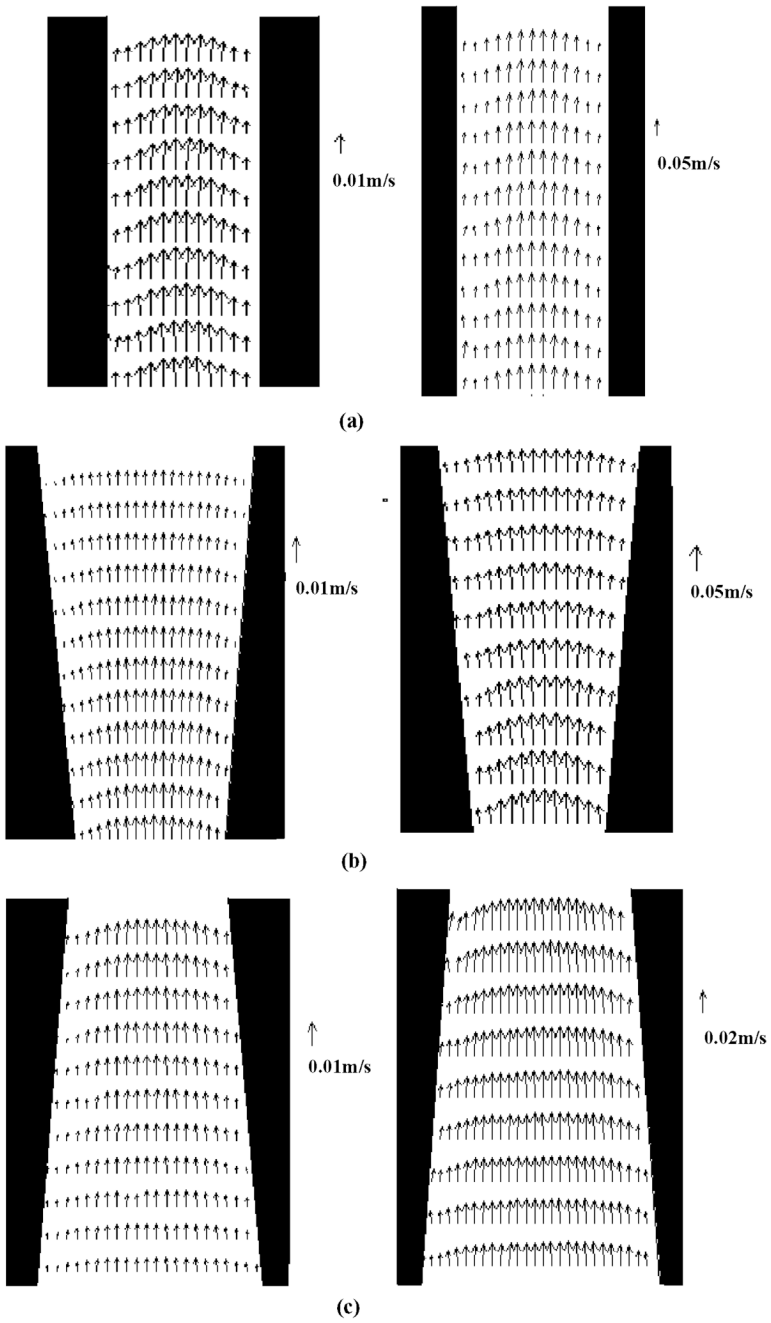

Fig. 8.

μ-PIV measurements taken at regions of the microchannel with (a) nonsloping wall profiles, (b) expanding conduits, and (c) contracting conduits at flow rates of 1 μl/min and 5 μl/min.

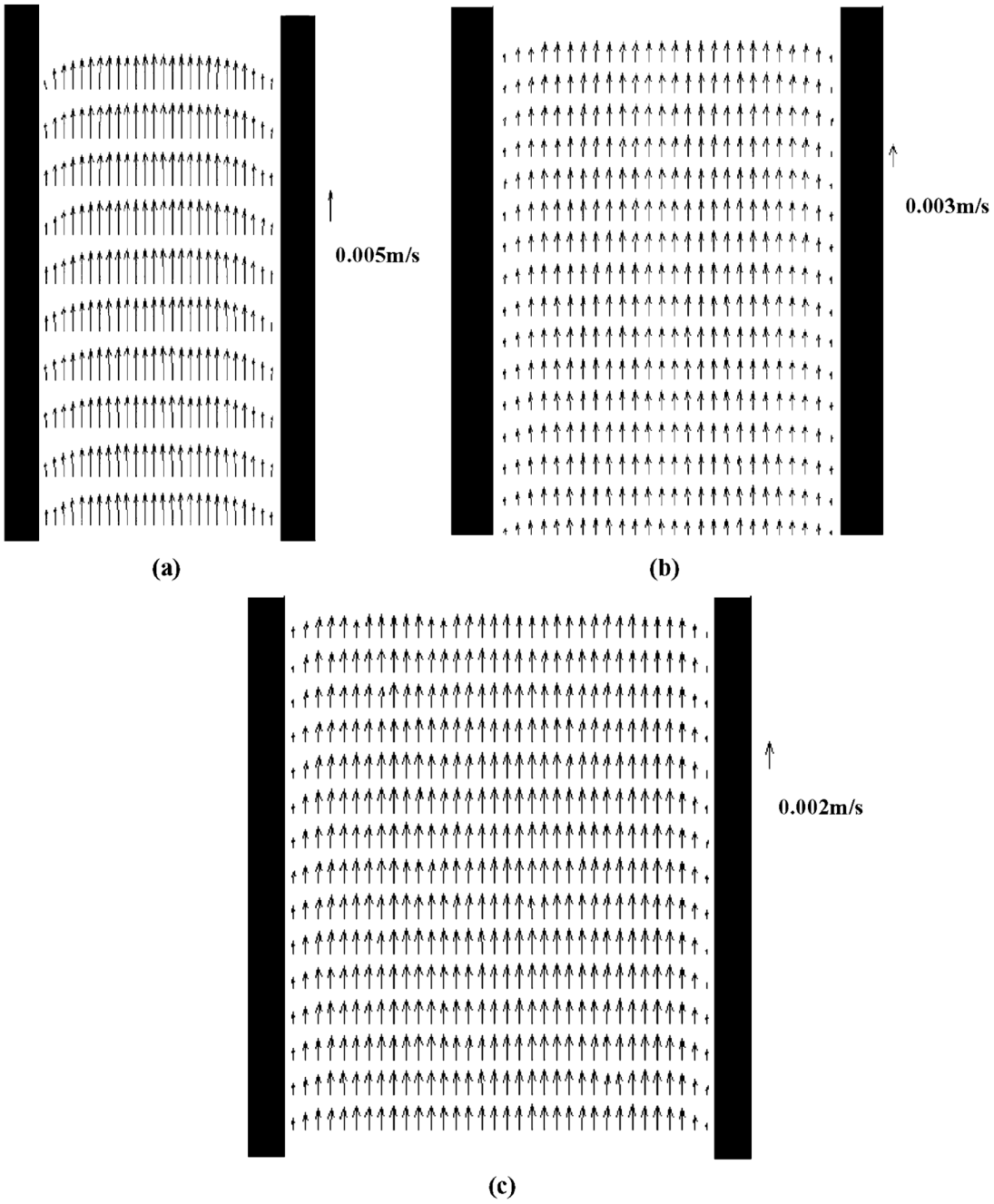

Fig. 9.
μ-PIV measurements taken at a segment of the microchannel in the (a) denaturation zone, (b) annealing zone, and (c) extension zone at the flow rate of 1 μl/min.

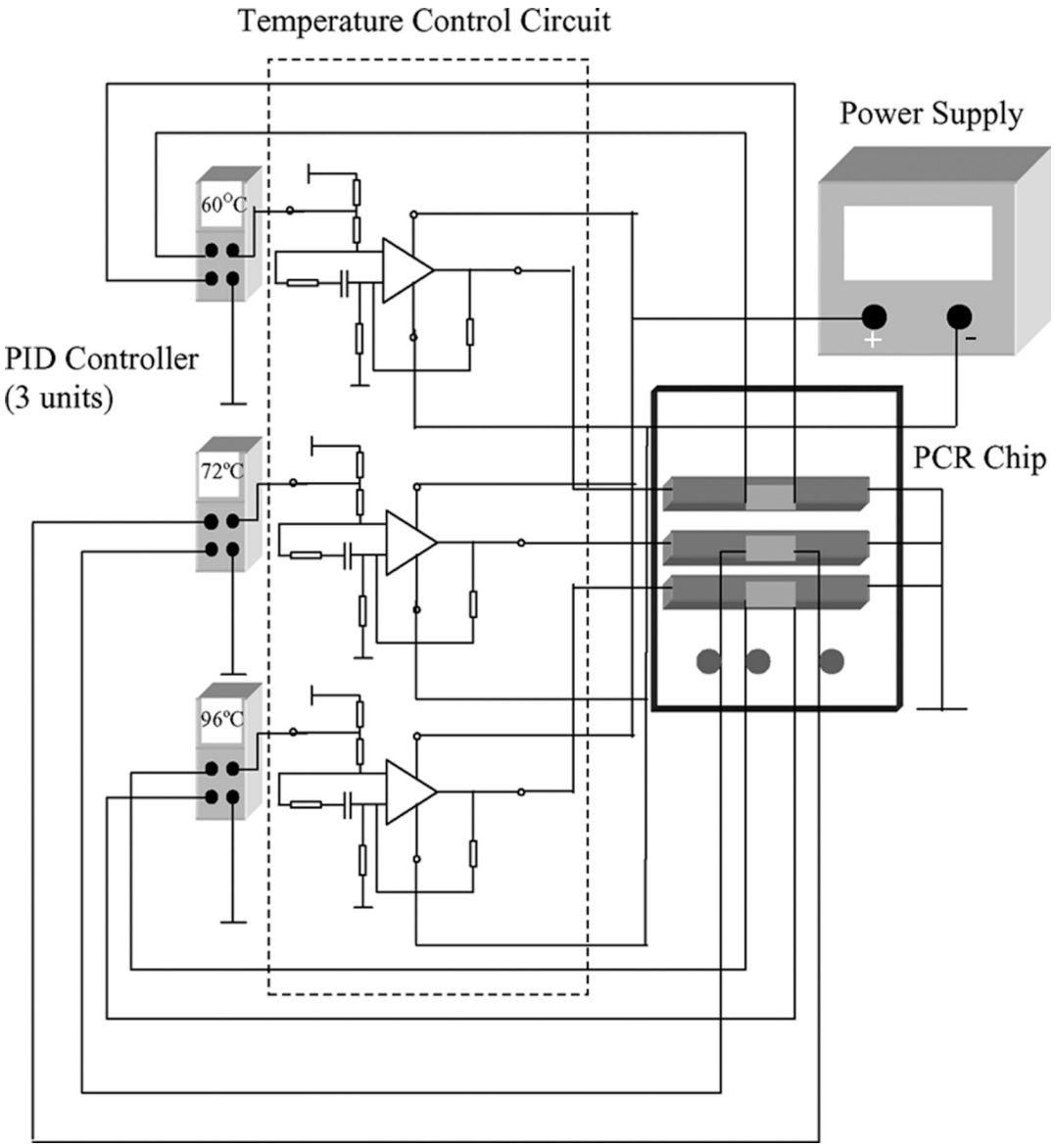

Fig. 10.
The experimental setup for running DNA amplification experiments and the wiring diagram of the temperature control system.

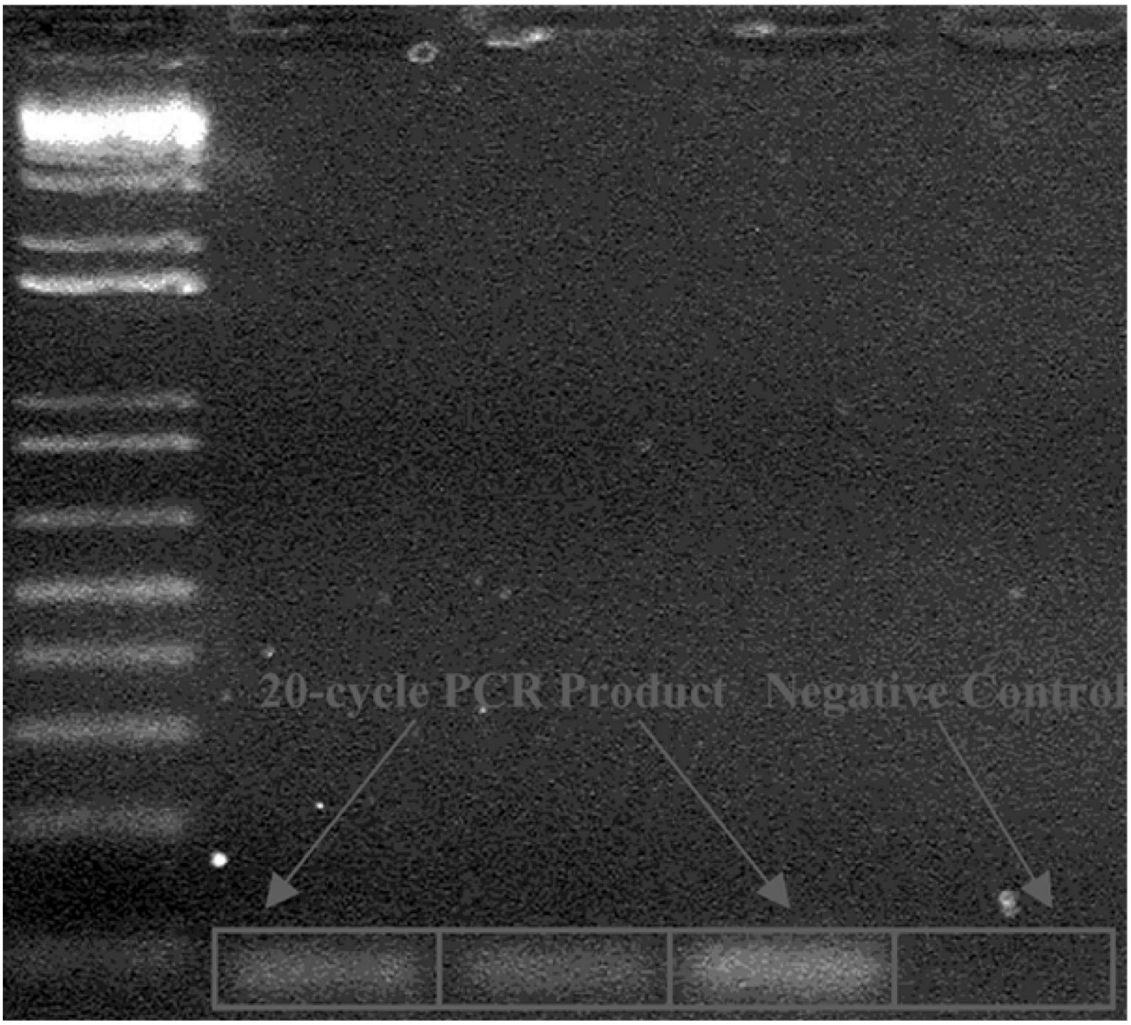

Fig. 11.
Gel electrophoresis results from a 20-cycle amplification reaction at 1 μl/min.